For an adiabatic turbulent boundary layer, the total temperature gradients are negligible and we may neglect total temperature fluctuations. Hence the hot wire sensitivity becomes,

$$\tilde{e}/e = S_{\rho u}\,(\tilde{\rho}u/\rho u)$$

Results

The momentum thickness Reynolds number for the test section roof was measured to be between 0.3×10^4 and 1.6×10^4. This compares with a typical value of $R_\theta \simeq 10^4$ measured at the trailing edge of models in larger test facilities. The pressure gradient parameter $\beta=\delta^*(dp/dx)_w$ was within ±0.015. The values of $\tilde{p}/q$ ranged from 0.003, comparable with the noise levels in well designed closed tunnels,[2] to 0.026, representing the noisy environment typical of many large ventilated tunnels.

Using the notation adopted by Mabey,[2] some typical pressure fluctuation spectra are presented in Fig. 1 for a typical test Mach number of 0.78 and one value of $R_\theta = 1.5\times10^4$. For the double slotted liner, the peak amplitude varies from $\sqrt{nF(n)}=0.20$ at $n=0.6$ to $\sqrt{nF(n)}=0.22$ at $n=0.9$, while for the single slotted liner with the perforated screens, the peak amplitude varies from $\sqrt{nF(n)}=0.03$ at $n=3.2$ to $\sqrt{nF(n)}=0.08$ at $n=4$.

Figure 2 shows the small influence of pressure fluctuations on the boundary-layer shape factor H, and Fig. 3 shows the small influence on the skin friction coefficient C_f for a typical value of R_θ. The skin friction coefficient was obtained from the log of the wall plot for compressible turbulent boundary layers. These changes in R_θ, C_f, and H due to pressure fluctuations are an order less than those due to pure velocity fluctuations observed in low speed flows.

Figure 4 shows the typical variation of velocity and density fluctuations in the boundary layer with changes in the pressure fluctuation levels. It can be seen that a large increase in $\tilde{p}/q$ from 0.0055 to 0.0226 produces a significant increase in $\tilde{u}/u$ and $\tilde{\rho}/\rho$ over a large portion of the boundary layer. The general distribution of $\tilde{u}/u$ in the boundary layer is similar to that measured in a low speed boundary layer ($U=10$ m/s) with a freestream turbulence level of 2.4%.[3] The temperature or density fluctuations are an order less than the velocity fluctuations and do not show the same degree of variation as $\tilde{u}/u$ but tend to have a nearly constant value through the boundary layer.

Thus, for small pressure gradients and attached flow, the turbulence within the turbulent boundary layer is significantly influenced by the external pressure fluctuations, but the corresponding changes in the mean properties of the boundary layer are fairly small.

Acknowledgment

This work originated as part of the research supported by S.R.C. Contract B/RG/8932.

References

[1] "Fluid Motion Problems in Wind Tunnel Design," AGARD Rept. No. 602.

[2] Mabey, D. G., "Flow Unsteadiness and Model Vibration in Wind Tunnels at Subsonic and Transonic Speed," Aeronautical Research Council, ARC CP 1155.

[3] Charney, G., Comte-Ballot, G., and Mathieu, J., "Development of a Boundary Layer on a Flat Plate in an External Turbulent Flow," Paper No. 27, AGARD CP-93, 1971.

[4] Green, J. E., "On the Influence of Free Stream Turbulence on a Turbulent Boundary Layer, as it Relates to Wind Tunnel Testing at Subsonic Speeds," *AGARD Rept. 602 on Fluid Motion Problems in Wind Tunnel Design*, 1973.

[5] Weeks, D. J. and Hodges, J., "An Experimental Investigation into the Influence of Acoustic Disturbances on the Development of a Turbulent Boundary Layer," RAE Tech. Rept. 77035; Royal Aircraft Establishment, Bedford, England.

[6] Ross, R. and Rohne, P. B., "The Character of Flow Unsteadiness and its Influence on Steady State Transonic Wind Tunnel Measurements," Paper 45, AGARD CP-174.

[7] Morkovin, M. V., "Fluctuations and Hot Wire Anemometry in Compressible Flows," AGARDograph, 24, Nov. 1956.

[8] Horstmann, C. C. and Rose, W. C., "Hot Wire Anemometry in Transonic Flows," NASA TM X-62, 495, 1975.

Numerical Solutions of Hypersonic Viscous Shock-Layer Equations

B. N. Srivastava,* M. J. Werle,† and R. T. Davis‡
University of Cincinnati, Cincinnati, Ohio

Nomenclature

n = coordinate measured normal to the body, nondimensionalized by the body nose radius
n_s = shock standoff distance
s = nondimensional surface distance coordinate
u = nondimensional velocity component tangent to the body surface
v = nondimensional velocity component normal to the body surface
η = transformed normal coordinate, normalized with value behind the shock
ξ = transformed surface coordinate, $\xi = s$

I. Introduction

THERE have been several efforts in the past to seek numerical solutions of hypersonic viscous shock-layer equations for reentry blunt-body applications.[1-3] Continued interest is motivated by the several advantages of using these equations[1] as compared to others and their wide domain of applicability; that includes the Mach numbers and Reynolds numbers commonly encountered during re-entry conditions.[3] However, most shock-layer methods encounter numerical difficulties whenever shock-layer thickness becomes large.[1] This difficulty usually manifests itself as a divergent behavior in the relaxation scheme used to update the shock shape.[4] In an attempt to overcome this problem, the results of a new approach are presented here.

The viscous shock-layer equations as applicable to blunt bodies are parabolic-hyperbolic in nature;[1] however, the effect of the unknown shock shape is to introduce an elliptic-type behavior. When the shock-layer thickness is small, the blunt-body problem is apparently of weak elliptic nature leading to the success of the past shock-layer methods.[1] For thick shock layers, a numerical technique that properly accounts for the global effect of the shock shape on a blunt body must be adopted. An efficient way to achieve this would be to employ a technique normally applied to elliptic partial differential equations with a specified downstream boundary condition. A modified version of the alternating direction implicit (ADI) finite-difference scheme is used in the present technique in order to provide the global influence of the shock shape during the numerical integration scheme.[4]

Received June 26, 1978; revision received Aug. 14, 1978.

Index categories: Supersonic and Hypersonic Flow; Viscous Non-boundary-Layer Flows; Computational Methods.

*Research Engineer, Avco Everett Research Laboratory, Everett, Mass. Member AIAA.

†Currently, Chief, Gas Dynamics Section, United Technology Research Center, East Hartford, Conn. Member AIAA.

‡Head, Aerospace Engineering. Member AIAA.

II. Nature of the Problem

Due to the extremely complicated form of the governing system of viscous shock-layer equations,[1,5] it is instructional to consider a model problem for the purpose of establishing the basic approach to be used in solving the viscous shock-layer equations,

$$\frac{\partial u}{\partial s}+\frac{\partial v}{\partial n}=0 \tag{1a}$$

$$\frac{\partial^2 u}{\partial n^2}+a\frac{\partial p}{\partial s}=0 \tag{1b}$$

$$\frac{\partial p}{\partial n}+\epsilon\frac{\partial v}{\partial s}=0 \tag{1c}$$

with the associated boundary conditions at the surface and the shock locations are

$$u(s,0)=v(s,0)=0,\quad u(s,1)=v(s,1)=1,\text{ and } p(s,1)=p_e=cdn_e/ds \tag{2a}$$

where the last relation in Eq. (2a) is a consequence of Rankine-Hugoniot relations and

$$n_e=\int_0^1 u\,dn \tag{2b}$$

Equation (1a) is taken as a model of the continuity equation, Eq. (1b) models the longitudinal momentum equation, and Eq. (1c) models the normal momentum equation. a,c,ϵ are constants. Note that setting $\epsilon=0$ in Eq. (1c) is equivalent to invoking the thin shock-layer approximation.[1,4] An important point concerning these equations is that even though they appear to be of hyperbolic-parabolic type they actually have an "elliptic" nature through the dependence of the solution on the shock-layer thickness. To see this more clearly, it is first convenient to normalize the pressure with its edge value be defining $\bar{p}$ according to relation $\bar{p}=p/p_e$ so that Eq. (1b) now becomes

$$\frac{\partial^2 u}{\partial n^2}+ap_e\frac{\partial \bar{p}}{\partial s}+a\bar{p}\frac{\partial p}{\partial s}=0 \tag{3a}$$

Using the last of Eq. (2a) and (2b), this becomes

$$\frac{\partial^2 u}{\partial n^2}+ac\bar{p}\int_0^1\frac{\partial^2 u}{\partial s^2}\,dn+ap_e\frac{\partial \bar{p}}{\partial s}=0 \tag{3b}$$

The appearance of the second derivative of u with respect to the surface distance s under the integral was taken by Garvine[6] to signal the possible occurrence of "elliptic"-type behavior in these equations. As in elliptic problems, the second-order longitudinal derivative controls the fundamental nature of the problem and so long as coefficient $ac\bar{p}>0$ Eq. (3b) is an ill-posed initial value problem. A numerical technique for solving such problems is to introduce a time-like term in Eq. (3b) and thereby relaxing to the steady state while applying a boundary condition at the downstream boundary of the problem. Thus Eq. (3b) is written in the form

$$\frac{\partial^2 u}{\partial n^2}+ap_e\frac{\partial \bar{p}}{\partial s}+ac\bar{p}\left[\frac{\partial^2 n_e}{\partial s^2}-\frac{\partial n_e}{\partial t}\right]=0 \tag{4}$$

and some boundary conditions on n_e would be imposed at both ends of the region of interest as a forward march is performed in time.

III. The "Unsteady" Shock-Layer Equations and ADI Technique

The equations governing the viscous shock-layer concept will not be presented here since they are included in the papers cited.[1] However, in order to demonstrate the ADI concept as applicable to viscous shock-layer equations, it is relevant to present the final form of the longitudinal momentum and energy equations[4] as

$$\frac{\partial^2 \tilde{w}}{\partial \eta^2}+\alpha_1\frac{\partial \tilde{w}}{\partial \eta}+\left(\gamma_2\frac{\partial^2 n_s}{\partial s^2}+\gamma_2'\right)\tilde{w}+\left(\gamma_3\frac{\partial^2 n_s}{\partial s^2}+\gamma_3'\right)+\alpha_4\frac{\partial \tilde{w}}{\partial \xi}=0 \tag{5}$$

where $\tilde{w}$ represents normalized velocity $\tilde{u}$ for the longitudinal momentum equation and normalized temperature $\tilde{t}$ for the energy equation. The coefficients $\alpha_1,\gamma_2,\gamma_2',\gamma_3,\gamma_3'$, and α_4 are presented in Ref. 4. Note that Eq. (5) is similar to Eq. (3b) of the model problem and therefore a time-like technique as depicted by Eq. (4) of the model problem can be adopted for the solution of the viscous shock-layer equations. The technique is essentially a two-time step process in which the first step is used to determine the flow parameters across the shock layer while marching from the stagnation point to the end of the flow region of interest. During the second time step the shock-layer thickness n_s itself is determined by solving Eq. (5) along a single line parallel to the body surface. The two-step process is depicted by the following equations.

First step $t^*=t^n+\Delta t/2$

$$\frac{\partial^2 \tilde{w}^*}{\partial \eta^2}+\alpha_1^*\frac{\partial \tilde{w}^*}{\partial \eta}+\left[\gamma_2^*\left(\frac{\partial^2 n_s^n}{\partial s^2}-\frac{n^*-n^n}{\Delta t/2}\right)+\gamma_2'^*\right]\tilde{w}^*+\left[\gamma_3^*\left(\frac{\partial^2 n_s^n}{\partial s^2}-\frac{n^*-n^n}{\Delta t/2}\right)+\gamma_3'^*\right]+\alpha_4^*\frac{\partial \tilde{w}^*}{\partial \xi}=0 \tag{6}$$

where superscript n represents the value of the quantity evaluated at the previous time step and * represents the current value.

Second Step $t^{n+1}=t^*+\Delta/t2$

$$\frac{\partial^2 n_s^{n+1}}{\partial^2 s^2}-\frac{n^{n+1}-n^*}{\Delta t/2}+\left(\frac{\partial^2 \tilde{w}^*}{\partial \eta^2}+\alpha_1^*\frac{\partial \tilde{w}^*}{\partial \eta}+\alpha_4\frac{\partial \tilde{w}^*}{\partial \xi}+\gamma_3'^*+\gamma_2'^*\tilde{w}^*\right)\Big/(\gamma_3^*+\gamma_2^*\tilde{w}^*)=0 \tag{7}$$

where superscript $n+1$ represents the value of the quantity at the current time step. Since the shock shape does not depend on the η variable, the final sweep equation is solved at one particular station in the η direction (here this solution was obtained at one grid point off the wall). However, this second sweep equation requires a statement of the boundary conditions for shock shape at the beginning and end of the finite-difference domain. The first of these is the symmetry condition at $s=0$, which leads to a derivative boundary condition on the shock shape, i.e., $(dn_s/ds)_{s=0}=0$. The proper placement of the downstream boundary condition causes some difficulty. Far downstream one would expect the shock to approach its inviscid configuration which could be determined either numerically or possibly analytically from hypersonic small disturbance theory. At the present time the mesh lengths being employed are too short to make use of the asymptotic shock shape and thus an approximate procedure is employed here. The shock thickness at the downstream end for the final sweep equation, n_s^{n+1}, is presently taken to be

that obtained from the first sweep solutions. Thus, for the final sweep the boundary conditions employed here are

$$s=0 \qquad \frac{dn_s}{ds}=0 \tag{8}$$

$$s=s_{\max}n \qquad {}^{n+1}_{s_{\max}} = n^{*}_{s_{\max}} \tag{9}$$

For the overall solution technique and further details of this method, one is referred to Ref. 4.

IV. Results and Discussion

One of the major difficulties encountered with previous shock-layer-methods[1,3] is that the success of such methods depends on a rather careful choice of the initial shock shape. In general an arbitrary choice of the initial shock shape leads to divergent behavior of such schemes. The present technique has been found to yield accurate numerical results with an arbitrary initial guess on the shock shape. This is demonstrated through Fig. 1 where numerical solutions are generated for flow past a hyperboloid asymptotic to a cone half angle of 22.5 deg at a freestream Mach number of 21.75, a freestream temperature, T_∞, of 351.8°R, and a surface temperature, T_w of 1800°R corresponding to a case considered by Davis.[7] A very crude guess on the initial shock shape was made by assuming the shock standoff distance to be 1 (nondimensionalized by nose radius) everywhere. Figure 1 shows the relaxation of the stagnation point shock standoff distance with time for various time step sizes Δt. Both a thin layer approximation as well as a full layer version of the shock-layer equations were used in this calculation. The transition from the thin layer version to the full layer version is marked by a "kink" following the converged state of the thin layer form. It is observed from this figure that fully converged solutions are obtained for both thin and full shock-layer equations with any arbitrary guess. The solutions so obtained were found to compare well with the previous method of Davis.[4] More detailed investigations of the present technique as compared to other shock-layer techniques[4] indicate that the current technique enjoys a greater degree of flexibility. In order to test the generality of the present technique, numerical solutions were generated for various blunt bodies corresponding to available experimental data. These results are presented in Figs. 2 and 3. Figure 2 shows the pressure distribution on a hyperboloid asymptotic to a cone half angle of 10 deg at a freestream Mach number of 10 and a hot wall case ($T_w/T_0 \simeq 0.9$) corresponding to the experimental data of Little.[8] It is observed that the comparison of the present technique with the technique of Davis[1] and the experimental data is good. However, when the hyperboloid cone half angle was reduced to 5 deg and below, the method of Davis[1] failed to converge due to large shock-layer thickness associated with such bodies, whereas the present technique yielded properly converged solutions. Finally, Fig. 3 shows

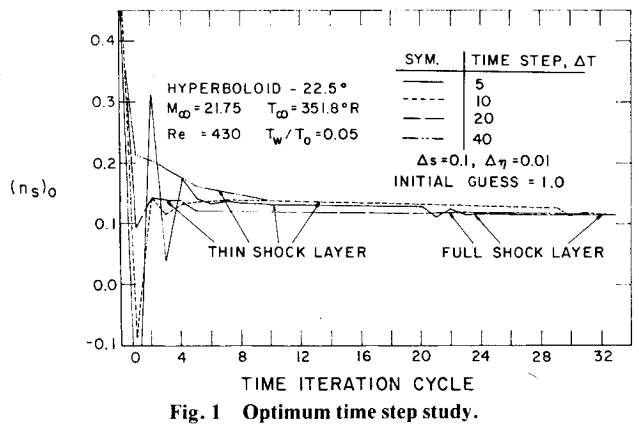

Fig. 1 Optimum time step study.

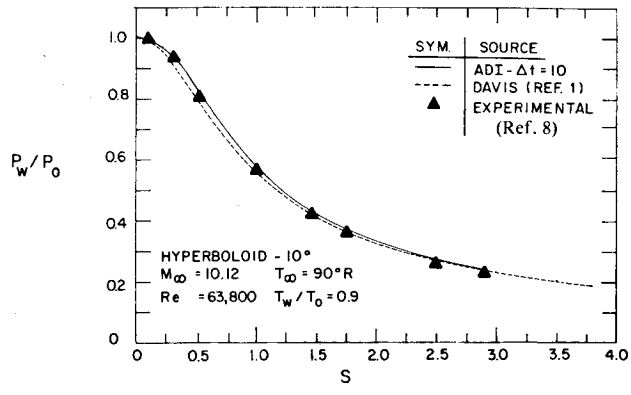

Fig. 2 Surface pressure comparisons with experimental data (hyperboloid).

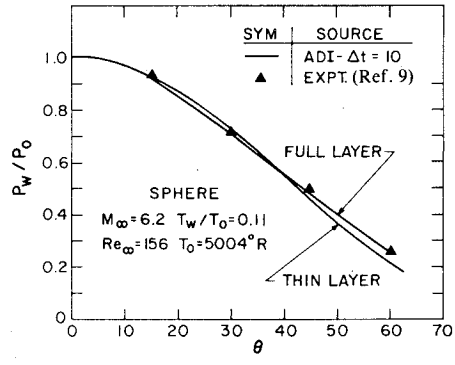

Fig. 3 Surface pressure comparisons with experimental data (sphere).

the pressure distribution over a spherical body corresponding to the experimental data of Bailey and Sims.[9] At this test condition it was found that the shock-layer thickness was large enough to warrant the use of the present technique for convergence. The numerical results using the present scheme are seen to compare well with the experimental data. The advantages of the present method are its general applicability to most blunt bodies generally encountered during reentry flights and greater flexibility in generating numerical solutions for such problems.

References

[1] Davis, R. T., "Numerical Solution of the Hypersonic-Viscous Shock Layer Equations," *AIAA Journal*, Vol. 8, May 1970, pp. 843-851.

[2] Srivastava, B. N., Werle, M. J., and Davis, R. T., "Solution of the Hypersonic Viscous Shock Layer Equations for Flow Past a Paraboloid," Dept. of Aerospace Engineering, University of Cincinnati, Cincinnati, Ohio, Rept. AFL-74-4-10, April 1974; also *AIAA Journal*, Vol. 14, Feb. 1976, pp. 257-259.

[3] Srivastava, B. N., Werle, M. J., and Davis, R. T., "Stagnation Region Solutions of the Full Viscous Shock-Layer Equations," *AIAA Journal*, Vol. 14, Feb. 1976, pp. 274-276; also Arnold Engineering Development Center, Tenn., Rept. AEDC-TR-76-53, Aug. 1976.

[4] Werle, M. J., Srivastava, B. N., and Davis, R. T., "Numerical Solutions to the Full Viscous Shock Layer Equations Using an ADI Technique," Department of Aerospace Engineering, University of Cincinnati, Cincinatti, Ohio, AFL 74-7-13, Aug. 1974.

[5] Srivastava, B. N., Werle, M. J., and Davis, R. .T., "Viscous Shock Layer Solutions for Hypersonic Sphere-Cones," *AIAA Journal*, Vol. 16, Feb. 1978, pp. 137-144.

[6] Garvine, R. W., "Upstream Influence in Viscous Interaction Problems," *The Physics of Fluids*, Vol. 11, July 1968, pp. 1413-1423.

[7] Davis, R. T., "Hypersonic Flow of a Chemically Reacting Binary Mixture Past a Blunt Body," AIAA Paper 70-805, 1970.

[8] Little, H. R., "An Experimental Investigation of Surface Conditions on Hyperboloid and Paraboloids at a Mach Number of 10," AEDC-TR-69-225, Jan. 1970.

[9]Bailey, A. B. and Sims, W. H., "The Shock Shape and Shock Detachment Distance for Spheres and Flat-Faced Bodies in Low Density, Hypervelocity Argon Flow," Arnold Engineering Development Center, Tenn., Rept. AEDC-TDR-63-21, 1963.

Application of Brittle Coatings to Graphite Fiber-Reinforced Plastics

R. Prabhakaran*
Indian Institute of Technology, Kanpur, India

Nomenclature

E = Young's modulus
G = shear modulus
K = ratio of compressive strength of brittle coating to its tensile strength
S = composite compliance
γ = shear strain
ϵ = normal strain
ν = Poisson's ratio
σ = normal stress
τ = shear stress
θ = angle between L and x directions
θ' = angle between L direction and calibration beam axis
ϕ = angle between major principal stress and major principal strain

Subscripts

$1,L$ = direction of major amount of reinforcement in the composite
$2,T$ = direction transverse to the L direction in the plane of the composite
t = threshold
x = direction of the major principal strain in the composite
y = direction of the minor principal strain in the composite

Superscripts

C = brittle coating
S = specimen or structure made of composite material
$*$ = at the time of failure of the brittle coating
$'$ = for the calibration beam axes

Introduction

THE brittle coating method of stress analysis has the advantage of being a whole field method. While the magnitudes of the stresses determined by this method are subject to considerable error due to the many variables influencing the coating behavior, the directions of the principal strains are obtained easily and accurately. The number of strain gages required for measurement of stress can be reduced by determination of the principal directions with a brittle coating. With the increasing use of structures fabricated from advanced composites such as graphite fiber-reinforced plastics, there is a need to update the conventional methods of experimental stress analysis. Photo-orthotropic-elasticity[1] is one such development.

Received March 8, 1978; revision received Aug. 7, 1978.

Index categories: Structural Composite Materials; Structural Statics.

*Assistant Professor, Dept. of Mechanical Engineering.

The stress transfer from a structure fabricated from a composite material to a brittle coating is examined here. The failure of the coating according to the Mohr theory of failure is studied and results are presented for the case of brittle coating applied to a unidirectionally reinforced graphite-epoxy composite structure.

Analysis

The most frequently employed relationship[2] for the interpretation of brittle coating data in the case of isotropic structures is the simple equation

$$\sigma_1^s = E^s \epsilon_t^* \tag{1}$$

This relationship totally neglects the biaxial effects due to σ_2^s. In calibration,

$$\sigma_2^s = 0, \quad \epsilon_2^s = -\nu^s \epsilon_1^s \tag{2}$$

However, in practice σ_2^s and ϵ_2^s may have any value with respect to σ_1^s and ϵ_1^s. The effect of some of the variables, such as the strength ratio K and the Poisson's ratio mismatch, on the failure of the coating is shown in Ref. 2.

When a brittle coating is applied to an anisotropic structure, the analysis proceeds on the same lines as in the case of the isotropic structure: the principal strain directions for the structure and for the coating are assumed to be the same, and the strains are assumed to be transmitted faithfully from the structure to the coating. The plane state of stress produced in the coating by the plane state of stress acting on the surface of the composite structure can be represented by

$$\sigma_x^c = \frac{E^c}{1-(\nu^c)^2}\left[\sigma_x^s (A + B\nu^c) + \sigma_y^s (B + D\nu^c)\right] \tag{3}$$

$$\sigma_y^c = \frac{E^c}{1-(\nu^c)^2}\left[\sigma_x^s (A\nu^c + B) + \sigma_y^s (B\nu^c + D)\right] \tag{4}$$

where

$$A = \overline{S_{11}} - \frac{\overline{S_{16}}}{\overline{S_{66}}}\overline{S_{16}}, \quad B = \overline{S_{12}} - \frac{\overline{S_{16}}}{\overline{S_{66}}}\overline{S_{26}}, \quad D = \overline{S_{22}} - \frac{\overline{S_{26}}}{\overline{S_{66}}}\overline{S_{26}} \tag{5}$$

and $\overline{S_{11}}$, $\overline{S_{12}}$,... etc., are the composite compliances transformed to the principal strain axes, making an angle θ with the material symmetry axes.

If the brittle coating calibration is performed in the usual manner on beams prepared from the same composite material as the structure, with the angle between the beam axis and the direction of major reinforcement varied from 0 to 90 deg, we can write

$$\sigma_{x'}^s = \epsilon_{x'}^s / \overline{S_{11}'}, \quad \sigma_{y'}^s = 0 \text{ and } \epsilon_{x'}^s = \epsilon_t^* \tag{6}$$

Substituting Eqs. (6) in Eqs. (3) and (4), the coating stresses in the calibration beam are given by

$$\sigma_x^c = \frac{E^c}{1-(\nu^c)^2}\left[(A + B\nu^c)\sigma_x^*\right] \tag{7}$$

$$\sigma_y^c = \frac{E^c}{1-(\nu^c)^2}\left[(A\nu^c + B)\sigma_x^*\right] \tag{8}$$